Hybrid Molecular Materials Based upon Organic π-Electron Donors and Metal Complexes. Radical Salts of Bis(ethylenethia)tetrathiafulvalene (BET-TTF) with the Octahedral Anions Hexacyanoferrate(III) and Nitroprusside. The First Kappa Phase in the BET-TTF Family

Miguel Clemente-León,[†] Eugenio Coronado,*[,†] José R. Galán-Mascarós,[†] Carlos Giménez-Saiz,[†] Carlos J. Gómez-García,[†] Elisabet Ribera,[‡] José Vidal-Gancedo,[‡] Concepció Rovira,*[,‡] E. Canadell,[‡] and Vladimir Laukhin[‡,§]

Instituto de Ciencia Molecular, Universidad de Valencia, Dr. Moliner 50, 46100 Burjasot, Spain, and Institut de Ciència de Materials de Barcelona (CSIC), Campus Universitari de Bellaterra, 08193 Cerdanyola, Spain

Received December 20, 2000

The synthesis, structure, and physical characterization of two new radical salts formed with the organic donor bis(ethylenethia)tetrathiafulvalene (BET-TTF) and the octahedral anions hexacyanoferrate(III), $[Fe(CN)_6]^{3-}$, and nitroprusside, $[Fe(CN)_5NO]^{2-}$, are reported. These salts are $(BET\text{-}TTF)_4(NEt_4)_2[Fe(CN)_6]$ (**1**) (monoclinic space group $C2/c$ with $a = 38.867(7)$ Å, $b = 8.438(8)$ Å, $c = 11.239(6)$ Å, $\beta = 90.994(9)°$, $V = 3685(4)$ Å^3, $Z = 4$) and $(BET\text{-}TTF)_2[Fe(CN)_5NO]\cdot CH_2Cl_2$ (**2**) (monoclinic space group $C2/c$ with $a = 16.237(6)$ Å, $b = 18.097(8)$ Å, $c = 12.663(7)$ Å, $\beta = 106.016(9)°$, $V = 3576(3)$ Å^3, $Z = 4$). In salt **1** the organic BET-TTF molecules are packed in orthogonal dimers, forming the first kappa phase observed for this donor. The analysis of the bond distances and the electronic and IR spectra suggests a degree of ionicity of 1/4 per BET-TTF molecule, in agreement with the stoichiometry of the salt. The electrical properties show that **1** is a semiconductor with a high room-temperature conductivity (11.6 S cm^{-1}) and a low activation energy (45 meV), in agreement with the band structure calculations. The magnetic susceptibility of **1** shows, besides the paramagnetic contribution from the anion, a temperature-independent paramagnetism (TIP) of the Pauli type due to the electronic delocalization observed at high temperatures in the organic sublattice. This Pauli type paramagnetism is confirmed by the ESR spectra that also show a Dysonian line when the magnetic field is parallel to the conducting plane, typical of metallic and highly conducting systems. Salt **2** presents an unprecedented packing of the organic molecules that form zigzag tunnels where the anions and the solvent molecules are located. The stoichiometry indicates that all the BET-TTF molecules bear a charge of +1, and accordingly, **2** behaves as a semiconductor with a very low room-temperature conductivity. The magnetic properties of this salt indicate that the unpaired electrons on the organic molecules are strongly antiferromagnetically coupled, giving rise to a diamagnetic behavior of **2**, as the nitroprusside anion is also diamagnetic.

Introduction

The design and synthesis of molecular materials combining two or more physical properties as conducting, magnetic, and optical ones has become one of the most appealing challenges in the chemistry of materials in the past few years. An attractive approach to this goal is to make two-network solids by combining magnetic anions, which provide localized magnetic moments, with partially oxidized organic π-electron donor molecules of the tetrathiafulvalene (TTF) family, which support electronic conduction. This approach has already led to the preparation of many molecular semiconductors,[1] some metals,[2] and a few superconductors.[3] One of the advantages of this approach is the huge number of anions containing localized magnetic moments that can be used: from simple monoanions such as $[FeCl_4]^-$, which has been extensively used with TTF type donors,[2b,3b,4] to bulky magnetic polyoxometalates, which may also play an important structural role.[5] Between these two limits it is also possible to use magnetic monomeric anions with higher charges such as $[MX_4]^{2-}$ (M = Mn, Co, Ni, and Cu; X = Cl, Br),[2a,6] $[M(ox)_3]^{3-}$ (M = Fe, Cr, Co),[3a,7] and

* Corresponding authors. E-mail: eugenio.coronado@UV.es; c.rovira@icmab.es.

[†] Universidad de Valencia.

[‡] Institut de Ciència de Materials de Barcelona.

[§] Permanent address: Institute of Problems of Chemical Physics, 142432 Chernogolovka, MD, Russia.

(1) See for example: (a) Macéno, G.; Garrigou-Lagrange, C.; Delhaes, P.; Bechtel, F.; Bravic, G.; Gaultier, J.; Lequan, M.; Lequan, R. M. *Synth. Met.* **1988**, *27*, B57. (b) Kurmoo, M.; Day, P. Allan, M. Friend, R. H. *Mol. Cryst. Liq. Cryst.* **1993**, *234*, 199.

(2) (a) Day, P.; Kurmoo, M.; Mallah, T.; Marsden, I. R.; Friend, R. H.; Pratt, F. L.; Hayes, W.; Chasseau, D.; Gaultier, J.; Bravic, G.; Ducasse. L. *J. Am. Chem. Soc.* **1992**, *114*, 10722. (b) Coronado, E.; Falvello, L. R.; Galán-Mascarós, J. R.; Giménez-Saiz, C.; Gómez-García, C. J.; Laukhin, V. N.; Pérez-Benítez, A.; Rovira, C.; Veciana, J. *Adv. Mater.* **1997**, *9*, 984.

(3) (a) Kurmoo, M.; Graham, A. W.; Day, P.; Coles, S. J.; Hurtshouse, M. B.; Caulfield, J. L.; Singleton, J.; Pratt, F. L.; Hayes, W.; Ducasse, L.; Guionneau, P. *J. Am. Chem. Soc.* **1995**, *117*, 12209. (b) Kobayashi, H.; Tomita, H.; Naito, T.; Kobayashi, A.; Sakai, F.; Watanabe, T.; Cassoux, P. *J. Am. Chem. Soc.* **1996**, *118*, 368.

(4) (a) Kobayashi, A.; Udagawa, T.; Tomita, H.; Naito, T.; Kobayashi, H. *Chem. Lett.* **1993**, 2179. (b) Kumai, R.; Asamitsu, A.; Tokura, Y. *Chem. Lett.* **1996**, 753. (c) Batail, P.; Ouahab, L.; Torrance, J. B.; Pylman, M. L.; Parkin, S. S. P. *Solid State Commun.* **1985**, *55*, 597. (d) Kumai, R.; Asamitsu, A.; Tokura, Y. *Synth. Met.* **1997**, *85*, 1681. (e) Mallah, T.; Hollis, C.; Bott, S.; Kurmoo, M.; Day, P.; Allan, M.; Friend, R. *J. Chem. Soc., Dalton Trans.* **1990**, 859.

(5) Coronado, E.; Gómez-García, C. J. *Chem. Rev.* **1998**, *98*, 273, and references therein.

10.1021/ic001431l CCC: $20.00
Published on Web 06/08/2001

Table 1. Synthesis Conditions for the Radical Salts (BET-TTF)$_4$(NEt$_4$)$_2$[Fe(CN)$_6$] (**1**) and (BET-TTF)$_2$[Fe(CN)$_5$NO]·CH$_2$Cl$_2$ (**2**)

salt	anode	cathode
κ-(BET-TTF)$_4$(NEt$_4$)$_2$[Fe(CN)$_6$] (**1**)	BET-TTF (0.009 g)	
	(NEt$_4$)$_3$[Fe(CN)$_6$] (0.09 g)	(NEt$_4$)$_3$[Fe(CN)$_6$] (0.09 g)
	CH$_2$Cl$_2$ (6 mL)	CH$_2$Cl$_2$ (6 mL)
	CH$_3$CN (5 mL)	CH$_3$CN (5 mL)
(BET-TTF)$_2$[Fe(CN)$_5$NO]·CH$_2$Cl$_2$ (**2**)	BET-TTF (0.007 g)	
	K$_2$[Fe(CN)$_5$NO] (0.1 g)	K$_2$[Fe(CN)$_5$NO] (0.1 g)
	crown ether (0.15 g)	crown ether (0.15 g)
	CH$_2$Cl$_2$ (10 mL)	CH$_2$Cl$_2$ (10 mL)

[M(CN)$_6$]$^{3-}$ (M = Fe, Cr).[8] A more interesting magnetic component is furnished by the ferro- and ferrimagnetic and canted antiferromagnetic bimetallic oxalate layers of formula [M^{III}M^{II}(ox)$_3$]$^-$ (M^{III} = Fe, Cr, and Ru; M^{II} = Mn, Fe, Co, Ni, and Cu).[9] This family of molecule-based magnets has very recently been used with the organic donor bis(ethylenedithio)-tetrathiafulvalene (BEDT-TTF) to give the first molecular metallic ferromagnet.[10] Another possibility offered by the TTF family of organic donors is the combination of electrical conductivity with optical properties. This goal can be achieved by using the photochromic nitroprusside anion [Fe(CN)$_5$NO]$^{2-}$, which presents two light-induced long-lived metastable states when it is irradiated with light due to a bond isomerization of the NO group (that passes from N-bond (nitrosyl) to N−O (η^2) and to O-bond (isonitrosyl) coordination).[11] These isomerizations produce important geometrical changes in the anion that can be used to provoke light-induced changes in the TTF type counterions and, thus, in their conducting properties.[12]

Among the TTF type donors, one of the most promising molecules is the bis(ethylenethia)tetrethiafulvalene (BET-TTF), which presents two external rings with a S atom that enhances the side-to-side connectivity in the derived solids by S···S and C−H···S contacts, giving rise to packings with marked two-dimensional character. Many of the BET-TTF derivatives also show 2D electronic character and, hence, high conductivities. In fact, this donor has already led to many semiconductors and metals.[13]

Table 2. Crystal Data for the Radical Salts κ-(BET-TTF)$_4$(NEt$_4$)$_2$[Fe(CN)$_6$] (**1**) and (BET-TTF)$_2$[Fe(CN)$_5$NO]·CH$_2$Cl$_2$ (**2**)

	1	**2**
formula	C$_{62}$H$_{72}$FeN$_8$S$_{24}$	C$_{26}$H$_{18}$Cl$_2$FeN$_6$S$_{12}$O
a, Å	38.867(7)	16.237(6)
b, Å	8.438(8)	18.097(8)
c, Å	11.239(6)	12.663(7)
β, deg	90.994(9)	106.016(9)
V, Å^3	3685(4)	3576(3)
Z	4	4
fw	1754.61	941.95
space group	*C*2/*c*	*C*2/*c*
ρ_{calcd}, g cm^{-3}	1.545	1.749
λ, Å	0.71069	0.71069
μ, cm^{-1}	9.31	13.07
R^a	0.0754	0.0857
R_w	0.1711	0.2082

[a] $R = \sum(F_o - F_c)/\sum(F_o)$. [b] $R_w = [\sum[w(F_o^2 - F_c^2)^2]/\sum[w(F_o^2)^2]]^{1/2}$; $w = 1/[\sigma^2(F_o^2) + (0.2000P)^2]$, where $P = (F_o^2 + 2F_c^2)/3$. [c] $R_w = [\sum[w(F_o^2 - F_c^2)^2]/\sum[w(F_o^2)^2]]^{1/2}$; $w = 1/[\sigma^2(F_o^2) + (0.1364P)^2]$, where $P = (F_o^2 + 2F_c^2)/3$.

In this context, here we report on the synthesis and structural and physical characterization of two new radical salts prepared with the donor bis(ethylenethia)tetrathiafulvalene (BET-TTF) and the paramagnetic hexacyanoferrate(III), [Fe(CN)$_6$]$^{3-}$, anion, (BET-TTF)$_4$(NEt$_4$)$_2$[Fe(CN)$_6$] (**1**), and the nitroprusside anion, [Fe(CN)$_5$NO]$^{2-}$, (BET-TTF)$_2$[Fe(CN)$_5$NO]·CH$_2$Cl$_2$ (**2**).

Experimental Section

Synthesis of the Radical Salts. Both radical salts were synthesized on a platinum wire electrode by the standard electrochemical oxidation of the donor in a U-shaped cell under low constant current ($I = 1-1.2$ μA). The crystallization times vary from three to 10 days, depending on the salt. The exact conditions for the synthesis of the radical salts are summarized in Table 1.

X-ray Crystallographic Analysis. The crystal structure analyses were done on a black, shiny, long, platelike single crystal of **1** and on a black needlelike single crystal of **2** (approximate dimensions: 0.40 × 0.20 × 0.03 mm^3 and 0.30 × 0.15 × 0.04 mm^3, respectively). Relevant crystallographic data and structure determination parameters for the two salts are given in Table 2. The atomic coordinates, thermal parameters, and bond distances and bond angles of the asymmetric unit of the two salts are given in the Supporting Information. Cell parameters were obtained by the least-squares refinement method with 25 reflections in the two structures. Intensity data were measured at room

(6) See, for example: (a) Lequan, M.; Lequan, R. M.; Hauw, C.; Gaultier, J.; Maceno, G.; Delhaes, P. *Synth. Met.* **1987**, *19*, 409. (b) Lequan, M.; Lequan, R. M.; Maceno, G. Delhaes, P. *J. Chem. Soc., Chem. Commun.* **1988**, 174. (c) Marsden, I. R.; Allan, M. L.; Friend, R. H.; Kurmoo, M.; Kanazawa, D.; Day, P.; Bravic, G.; Chasseau, D.; Ducasse, L.; Hayes, W. *Phys. Rev. B* **1994**, *50*, 2118.

(7) (a) Martin, L.; Turner, S. S.; Day, P. *Synth. Met.* **1999**, *102*, 1638. (b) Coronado, E.; Galán-Mascarós, J. R.; Gómez García, C. J. *J. Chem. Soc., Dalton Trans.* **2000**, 205.

(8) (a) Bouherour, S.; Ouahab, L.; Peña, O.; Padiou, J.; Grandjean, D. *Acta Crystallogr.* **1989**, *C45*, 371. (b) Le Magueres, P.; Ouahab, L.; Briard, P.; Even, J.; Bertault, M.; Toupet, L.; Ramos, J.; Gómez-García, C. J.; Delhaes, P. *Mol. Cryst. Liq. Cryst.* **1997**, *305*, 479. (c) Clemente-León, M.; Coronado, E.; Galán -Mascarós, J. R.; Gómez-García, C. J.; Rovira, C.; Laukhin, V. N. *Synth. Met.* **1999**, *103*, 2339.

(9) (a) Tamaki, H.; Zhong, Z. J.; Matsumoto, N.; Kida, S.; Koikawa, M.; Achiwa, N.; Hashimoto, Y.; Okawa, H. *J. Am. Chem. Soc.* **1992**, *114*, 6974. (b) Clemente-León, M.; Coronado, E.; Galán Mascarós, J. R.; Gómez-García, C. J. *Chem. Commun.* **1997**, 1727. (b) Coronado, E.; Galán-Mascarós, J. R.; Gómez-García, C. J.; Ensling, J.; Gütlich, P. *Chem. Eur. J.* **2000**, *6*, 552.

(10) Coronado, E.; Galán-Mascarós, J. R.; Gómez-García, C. J.; Laukhin, V. N. *Nature* **2000**, *408*, 447.

(11) Carducci, M. D.; Pressprich, M. R.; Coppens, P. *J. Am. Chem. Soc.* **1997**, *119*, 2669.

(12) (a) Yu, H.; Zhu, D. *Physica C* **1997**, *282−287*, 1893. (b) Gener, M.; Canadell, E.; Khasanov, S. S.; Zorina, L. V.; Shibaeva, R. P.; Kushch, L. A.; Yagubskii, E. B. *Solid State Commun.* **1999**, *111*, 329. (c) Kushch, L.; Buravov, L.; Tkacheva, V.; Yagubskii, E.; Zorina, L.; Khasanov, S.; Shibaeva, R. *Synth. Met.* **1999**, *102*, 1646. (d) Clemente-León, M.; Coronado, E.; Galán-Mascarós, J. R.; Giménez-Saiz, C.; Gómez-García, C. J.; Fabre, J. M. *Synth. Met.* **1999**, *103*, 2279. (e) Clemente-León, M.; Coronado, E.; Galán-Mascarós, J. R.; Gómez-García, C. J.; Canadell, E. *Inorg. Chem.* **2000**, *39*, 5394.

(13) (a) Tarrés, J.; Veciana, J.; Rovira, C. *Synth. Met.* **1995**, *70*, 1167. (b) Tarrés, J.; Santaló, N.; Mas, M.; Molins, E.; Veciana, J.; Rovira, C.; Yang, S.; Lee, H.; Cowan, D. O.; Doublet, M. L.; Canadell, E. *Chem. Mater.* **1995**, *7*, 1558. (c) Rovira, C.; Tarrés, J.; Ribera, E.; Veciana, J.; Canadell, E.; Molins, E.; Mas, M.; Laukhin, V.; Doublet, M. L.; Cowan, D. O.; Yang, S. *Synth. Met.* **1997**, *86*, 2145. (d) Pérez-Benítez, A.; Rovira, C.; Veciana, J.; Vidal-Gancedo, J.; Laukhin, V. N.; Zorina, L. V.; Khasanov, S. S.; Narymbetov, B. Zh.; Shibaeva, R. P. *Synth. Met.* **1999**, *102*, 1707. (e) Laukhina, E. Ribera, E.; Vidal-Gancedo, J.; Khasanov, S. S.; Zorina, L. V.; Shibaeva, R.; Canadell, E.; Laukhin, V.; Honold, M.; Nam, M. S.; Singleton, J.; Veciana, J.; Rovira, C. *Adv. Mater.* **2000**, *12*, 54.

temperature on an Enraf-Nonius CAD4 diffractometer with graphite-monochromated Mo Kα radiation with the $\omega-2\theta$ method. The measurement of three standard reflections every 120 min revealed no intensity fluctuations. The structures were solved by direct methods using the SIR97 program,[14] followed by Fourier synthesis, and refined on F^2 using the SHELXL-97 program.[15] Lorentz, polarization, and semiempirical absorption corrections (ψ-scan method) were applied to the intensity data. All calculations were performed in a SPARC station 20 (Sun Microsystems). In **1** all the atoms, except some C, the N, and the H atoms, were refined anisotropically. In **2** only the heavy atoms (Fe and S) were refined anisotropically.

Conductivity Measurements. Direct current conductivity measurements over the range 25−300 K were performed with the standard four-contacts method for **1** and with two contacts for **2** on the best developed face of several single crystals of each sample, giving reproducible results in all cases. Contacts to the crystals were made by platinum wires (20 μm diameter) attached by graphite paste to the samples.

Magnetic Measurements. Variable-temperature susceptibility measurements were carried out in the temperature range 2−300 K at a magnetic field of 1 T on polycrystalline samples with a magnetometer (Quantum Design MPMS-XL-5) equipped with a SQUID sensor. The susceptibility data were corrected from the sample holders previously measured in the same conditions and from the diamagnetic contributions of the salts as deduced by using Pascal's constant tables. Variable-temperature ESR spectra were recorded on single crystals for **1** and on polycrystalline samples for **1** and **2** at X-band with Bruker ER200 and ER300 spectrometers equipped with helium cryostats and an automatic goniometer. The field was measured using a diphenylpicrylhydrazyl (DPPH, $g = 2.0036$) stable free radical marker.

Electronic and Vibrational Spectroscopies. Transmission measurements of pressed KBr pellets were recorded at room temperature with a Perkin-Elmer RX I FT-IR spectrophotometer in the range 400−6000 cm^{-1} and with a Hitachi U-2001 spectrophotometer in the range 9000−28000 cm^{-1} for compound **2**. For compound **1**, the measurements were made with a Perkin-Elmer Spectrum 1 FT-IR spectrophotometer in the range 400−7000 cm^{-1} and with a Varian Cary 5 spectrophotometer in the range 3333−20000 cm^{-1}.

Band Structure Calculations. The tight-binding band structure calculations used an extended Hückel-type Hamiltonian[16] and a modified Wolfsberg−Helmholtz formula[17] to calculate the nondiagonal H_{ij} matrix elements. Double-ζ orbitals[18] for C and S were used. The exponents and parameters employed in the calculations were taken from previous work.[19]

Results and Discussion

Synthesis and Structures. The radical salts were obtained by electrochemical oxidation of an organic solution containing neutral BET-TTF donor and the corresponding complex anion ($[Fe(CN)_6]^{3-}$ or $[Fe(CN)_5NO]^{2-}$). To make soluble these two anions, we have followed two different procedures. One involves the prior preparation of a tetraalkylammonium salt of the anion which is already soluble in the common organic solvents, while the other starts from a suspension of an alkaline salt (K^+ or Na^+) of the anion which is made soluble by addition of a crown ether such as the dibenzo[18]crown[6]. The use of the first strategy with the NEt_4^+ salt of the $[Fe(CN)_6]^{3-}$ anion led to shiny, black, long, platelike single crystals of the radical salt κ-(BET-TTF)$_4$(NEt_4)$_2$[$Fe(CN)_6$] (**1**), while the use of the second strategy led to very small, black, needlelike single crystals of a different phase whose structure has not been resolved yet. For the $[Fe(CN)_5NO]^{2-}$ anion, good quality black, needlelike single crystals of a radical salt formulated as (BET-TTF)$_2$[$Fe(CN)_5NO$]·CH_2Cl_2 (**2**) were obtained only when using the second strategy.

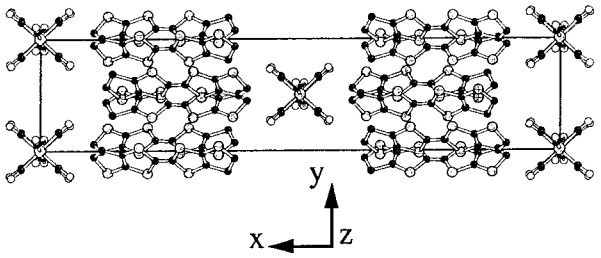

Figure 1. View of the *ab* plane showing the alternating organic and inorganic layers in κ-(BET-TTF)$_4$(NEt_4)$_2$[$Fe(CN)_6$] (**1**). The NEt_4^+ cations have been omitted for clarity.

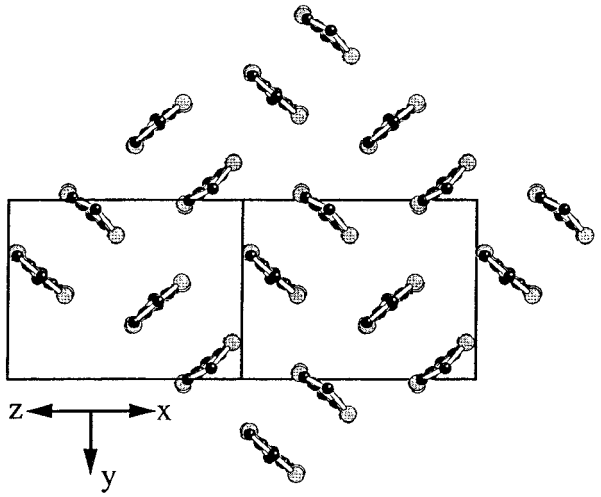

Figure 2. View of the organic layer in κ-(BET-TTF)$_4$(NEt_4)$_2$[$Fe(CN)_6$] (**1**) showing the κ packing of the BET-TTF molecules.

The crystal structures of **1** and **2** were determined by single-crystal X-ray analysis. The structure of **1** consists of layers of the organic donors alternating along the *a* axis with layers formed by the hexacyanoferrate anions and NEt_4^+ cations (Figure 1). The organic layer contains only one crystallographically independent BET-TTF molecule. The molecular arrangement in these layers consists of centrosymmetrical eclipsed dimers orthogonal to their closest dimers, giving rise to the well-known kappa phase (Figure 2).[20] Although this phase has already been observed in many radical salts with other TTF type donors (mainly BEDT-TTF), this is the first time this is observed for the BET-TTF donor. The intradimer S···S distances (shortest distance of 3.88 Å) are longer that the distances between orthogonal dimers (shortest distances of 3.76 and 3.80 Å) and similar to those observed between parallel dimers (shortest distance of 3.91 Å). These structural features support a marked two-dimensional character for the organic network. As there are two different organic layers per unit cell, a remarkable fact in this structure is the relative orientation of the dimers situated on consecutive layers (Figure 3). Thus, each dimer of a given

(14) SIR97: Altomare, A.; Burla, M. C.; Camalli, M.; Cascarano, G.; Giacovazzo, C.; Guagliardi, A.; Moliterni, A. G. G.; Polidori, G.; Spagna, R. *J. Appl. Crystallogr.* **1999**, *32*, 115.
(15) Sheldrick, G. M. *SHELXL-97*; University of Göttingen, 1997.
(16) (a) Whangbo, M.-H.; Hoffmann, R., *J. Am. Chem. Soc.* **1978**, *100*, 6093. (b) Hoffmann, R., *J. Chem. Phys.* **1963**, *39*, 1397.
(17) Ammeter, J.; Bürgi H.-B.; Thibeault, J.; Hoffmann, R. *J. Am. Chem. Soc.* **1978**, *100*, 3686.
(18) (a) Whangbo, M.-H.; Williams, J. M.; Leung, P. C. W.; Beno, M. A.; Emge, T. J.; Wang, H. H.; Carlson, K. D.; Crabtree, G. W. *J. Am. Chem. Soc.* **1985**, *107*, 5815. (b) Clementi, E.; Roetti, C., *At. Nucl. Data Tables* **1974**, *14*, 177.
(19) Pénicaud, A.; Boubekeur, K.; Batail, P.; Canadell, E.; Auban-Senzier, P.; Jérome, D. *J. Am. Chem. Soc.* **1993**, *115*, 4101.
(20) Williams, J. M.; Ferraro, J. R.; Thorn, R. J.; Carlson, K. D.; Geiser, U.; Wang, H. H.; Kini, A. M.; Whangbo, M. H. *Organic Superconductors. Synthesis, Structure, Properties and Theory*; Grimes, R. N., Ed.; Prentice Hall: Englewood Cliffs, NJ, 1992.

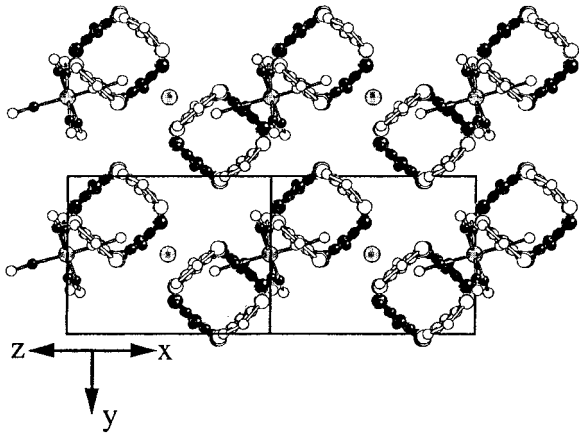

Figure 3. View of two consecutive organic layers (one in black and the other in white) and the inorganic one between them in the salt κ-(BET-TTF)$_4$(NEt$_4$)$_2$[Fe(CN)$_6$] (**1**). One of the two possible positions of the [Fe(CN)$_6$]$^{3-}$ anions is indicated only by the Fe atom.

layer is orthogonal to the closest dimer situated on the next layer in such a way that the projection of two consecutive layers gives rise to squares formed by two orthogonal dimers. Another relevant feature concerns the positional disorder found in the sulfur atoms of the two outer rings of the BET-TTF molecule. Thus, in one of the outer rings the S atom is statistically distributed over the two available positions (occupancy factor of 0.5), whereas in the other outer ring one of the positions is mainly occupied by a S atom (occupancy factor of 0.8) and the other by a C atom (occupancy factor of 0.8). This disorder, which has already been observed in other BET-TTF salts,[13,21] may arise from the coexistence of cis and trans isomers of the BET-TTF cations in the crystal due to an isomerization of the BET-TTF molecule (initially trans) during the oxidation process. A second contribution to the disorder may be due to the two possible ways of packing of the BET-TTF in the structure. The fact that the positional disorder is not completely statistical suggests a preferential packing mode of the BET-TTF cations, probably due to the tendency of these donors to maximize the intermolecular S···S interactions. Notice that the above disorder does not affect the central TTF skeleton of the BET-TTF, making it possible to roughly estimate its degree of ionicity from the bond distances in the central TTF fragment.[22] Assuming that the formulas developed for BEDT-TTF are valid for BET-TTF, we can estimate an average charge of +0.26 on each BET-TTF molecule, in good agreement with the calculated charge of +1/4 from the stoichiometry (4:1), the anionic charge (−3), and the presence of two NEt_4^+ cations.

The anionic layers are formed by discrete centrosymmetric [Fe(CN)$_6$]$^{3-}$ anions that exhibit a positional disorder along the *c* axis of the whole anion over two possible positions with an occupancy factor of 0.5. This disorder places the iron atoms at the origin of the unit cell (0,0,0) and at the center (1/2,1/2,1/2) or at the center of the *c* axis (0,0,1/2) and of the *ab* face (1/2,1/2,0) of the unit cell. In both cases the number of anions per unit cell is two and the iron atom always lies between two adjacent squares formed by two orthogonal dimers of consecutive layers (Figure 3). This disorder must come from a displacement of one-half of the anionic chains running along the *c* axis. The shortest Fe···Fe distances are equal to the *b* and

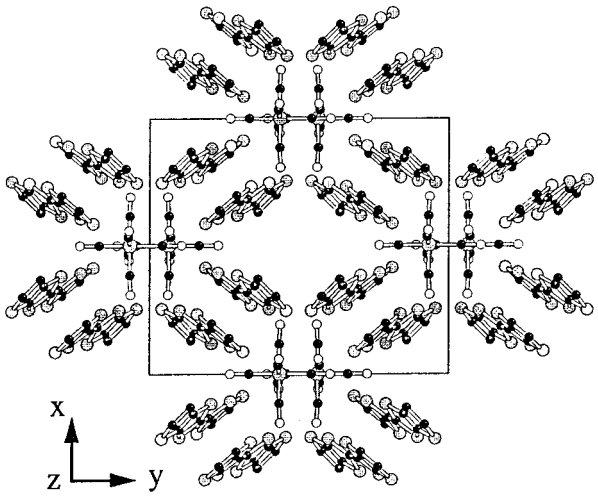

Figure 4. View of the *ab* plane showing the channels created by the BET-TTF dimers in (BET-TTF)$_2$[Fe(CN)$_5$NO].CH$_2$Cl$_2$ (**2**). The solvent molecules in the central channels have been omitted for clarity.

c parameters (8.438 and 11.239 Å, respectively). The Fe−C bond distances (1.91, 1.93, and 1.98 Å) are very similar to those found in the [Fe(CN)$_6$]$^{3-}$ anion (average Fe−C distance of 1.91 Å).[23] The [Fe(CN)$_6$]$^{3-}$ anions show some short contacts with the organic cations. Thus, the shortest N···C and N···S distances are 3.24 and 3.51 Å, respectively.

The structure of the nitroprusside derivative (**2**) is very unusual. Instead of exhibiting the typical segregated structure of organic layers alternating with layers of the inorganic anions, the organic network forms two types of zigzag channels running along the *c* axis. One of these channels accommodates the anions, while the solvent molecules (disordered water and possibly CH_2Cl_2) are located in the other channels (Figure 4). As in **1**, there is only one crystallographically independent BET-TTF molecule which is forming eclipsed pairs. A disorder between the external C and S atoms has also been observed. Thus, in the two disordered positions of the outer rings the C and S atoms appear, respectively, with multiplicities 0.5/0.5 in one of the external rings and 0.4/0.6 in the other. The BET-TTF molecules present several short intradimer S···S contacts (the shortest intradimer S···S distance is 3.30 Å). There are also some short S···S interdimer contacts (the shortest interdimer S···S distance is 3.50 Å). The low resolution of the structure and, hence, the high standard deviations in the bond distances preclude any estimation of the degree of ionicity of the BET-TTF molecule from its bond distances. Still, from the stoichiometry of the salt (2:1) and the charge of the complex anion (−2), it is clear that the BET-TTF molecules are fully ionized. This conclusion is supported by the electronic and magnetic properties (see below).

The inorganic anions are located inside the zigzag channels (Figures 4 and 5). The [Fe(CN)$_5$NO]$^{2+}$ anions appear as discrete anions located on a C_2 axis. The shortest intra- and interchannel Fe···Fe distances are 6.74 and 12.16 Å, respectively. There is a positional disorder in the NO^+ ligand which appears mainly delocalized over two of the six coordination positions of the iron atom. These two positions present Fe−C/N distances of 1.75(2) Å, which are between the expected values for the Fe−N and Fe−C bond distances observed in the ordered nitroprusside anion (1.65−67 and 1.91 Å, respectively). The other four Fe−C distances are longer (1.85(3), 1.85(4), 1.88(2), and 1.88(2) Å) and closer to the normal Fe−C bond distances (1.91 Å) in both

(21) Coronado, E.; Galán-Mascarós, J. R.; Giménez-Saiz, C.; Gómez-García, C. J.; Rovira, C.; Tarrés, J.; Triki, S.; Veciana, J. *J. Mater. Chem.* **1998**, *8*, 313.

(22) Guionneau, P.; Kepert, C. J.; Bravic, G.; Chasseau, D.; Truter, M. R.; Kurmoo, M.; Day, P. *Synth. Met.* **1997**, *86*, 1973.

(23) Le Magueres, P. Ph.D. Dissertation, University of Rennes, France, 1995.

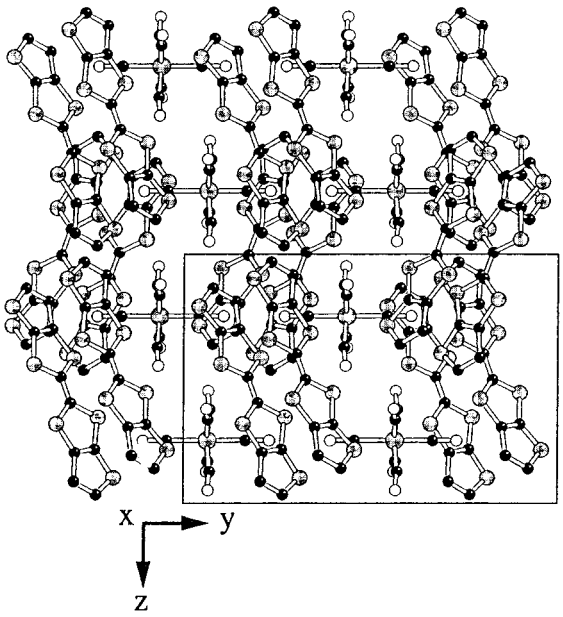

Figure 5. Side view of the zigzag channels running along the *c* axis in the salt (BET-TTF)$_2$[Fe(CN)$_5$NO]·CH$_2$Cl$_2$ (**2**).

the $[Fe(CN)_5NO]^{2-}$ and $[Fe(CN)_6]^{3-}$ anions.[24] There are many short anion−cation contacts (the shortest N···S distance is 2.92 Å), suggesting the existence of significant interactions between the BET-TTF molecules and the $[Fe(CN)_5NO]^{2-}$ anions.

Electronic and Vibrational Spectroscopies. The IR spectra of the two radical salts show the bands corresponding to the organic donor and to the anions. In the case of **1** the typical bands of the NEt_4^+ cations are also observed. In both salts the CN bands of the anions appear, as usually, in the 2050−2150 cm^{-1} region, while in **2** a band associated with the NO group is also observed at 1870 cm^{-1}. Let us focus on the vibrational stretching modes associated with the double C=C bonds of the central part of the BET-TTF molecule, which are sensitive to the degree of ionicity of the organic donor.[25] We observe that in **1** the ν_3 and ν_{27} bands appear at 1317 and 1433 cm^{-1}, respectively, while in **2** these bands are shifted toward higher energies (1341 and 1459 cm^{-1}) and are sharper. This result indicates a higher degree of ionicity of the BET-TTF molecules in **2**, in agreement with the charges deduced from the chemical formulas (+1/4 in **1** and +1 in **2**). A further support to this electron distribution comes from the differences observed in the vis−NIR spectra of **1** and **2**. In the spectrum of **1** we observe a broad and intense charge transfer band centered in the IR region at ca. 2700 cm^{-1} (the so-called A-band), which corresponds to electron transfers between neutral and completely charged donor molecules and is the signature of a mixed valence state in the organic network. In addition, we can also observe a weaker band at 11 700 cm^{-1} (the so-called B-band), which corresponds to electron transfers between donor molecules with an integer charge.[26] In contrast, the spectrum of **2** only shows a band of type B at 11 550 cm^{-1}, indicating that in this compound the BET-TTF molecules present an integer charge.

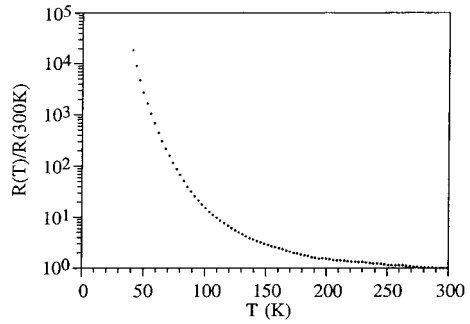

Figure 6. Thermal variation of the normalized resistance in a single crystal of the salt κ-(BET-TTF)$_4$(NEt$_4$)$_2$[Fe(CN)$_6$] (**1**).

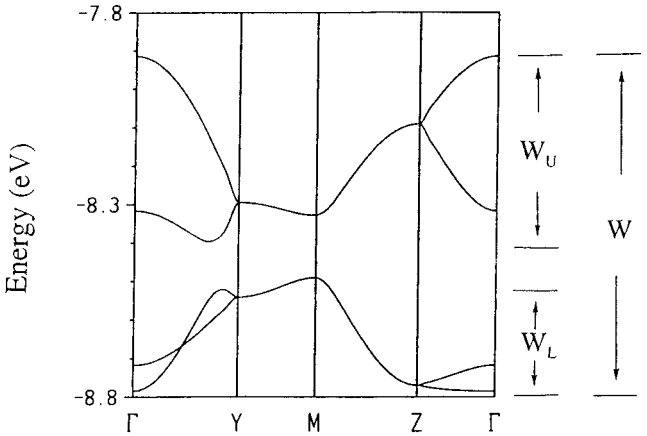

Figure 7. Calculated dispersion relations for the donor layers of κ-(BETTTF)$_4$(NEt$_4$)$_2$[Fe(CN)$_6$] (**1**) assuming an ordered layer of *cis*-BET-TTF donors. Γ = (0, 0), Y = (*b**/2, 0), Z = (0, *c**/2), and M = (*b**/2, *c**/2).

Electrical Properties. The temperature dependence of the normalized resistivity of **1**, measured in the bc plane of the crystals, which is parallel to the donor layers, is displayed in Figure 6. The room-temperature conductivity is 11.6 S cm^{-1}. The resistivity increases upon cooling the sample, indicating a semiconducting behavior even if the room-temperature conductivity is quite high. From a logarithmic plot of the resistivity we can estimate an activation energy of 45 meV. We can conclude that this salt is a semiconductor with a high room-temperature conductivity and a low activation energy. In contrast, **2** shows a very low room-temperature conductivity (<10^{-6} S cm^{-1}) and a strong electron localization. This is in agreement with the charge of +1 on the BET-TTF molecules and with the structural features.

Electronic Structure. Because of the above-mentioned structural disorder, we have considered several ordered models in studying the electronic structure of the donor layers of **1**. The dispersion relations calculated for the four highest occupied bands of an ordered layer of cis-BET-TTF donors are shown in Figure 7. These bands are mainly built from the HOMO of the BET-TTF donor. The double degeneracy of the bands along some directions of the Brillouin zone is due to the existence of nonsymmorphic symmetry elements. Since the unit cell contains four BET-TTF donors with an average charge of +1/4, there are seven electrons to fill the bands of Figure 7 so that the upper pair of bands should be one-quarter empty. The calculated values of W, W_L, and W_U (see Figure 7) which characterize the topology of the band structure of the κ-phases[27] are 0.88, 0.30, and 0.48

(24) (a) Shyu, H. L.; Wei, H. H.; Wang, Y. *Inorg. Chim. Acta* **1997**, *258*, 81. (b) Pressprich, M. R.; White, M. A.; Vekhter, Y.; Coppens, P. *J. Am. Chem. Soc.* **1994**, *116*, 5233.
(25) (a) Kozlov, M. E.; Pokhodnia, K. I.; Yurchenko, A. A. *Spectrochim. Acta* **1989**, *45A*, 437. (b) Swietlik, R.; Garrigou-Lagrange, C.; Sourisseau, C.; Pages, G.; Delhaès, P. *J. Mater. Chem.* **1992**, *2*, 857.
(26) Torrance, J. A.; Scot, B. A.; Welber, F. B. *Phys. Rev B* **1979**, *19*, 730.
(27) Jung, D.; Evain; M.; Novoa; J. J.; Whangbo, M.-H.; Beno, M. A.; Kini, A. M. Schultz, A. J.; Williams, J. M.; Nigrey, P. J. *Inorg, Chem.* **1989**, *28*, 4516.

eV, respectively. The corresponding values for an ordered layer of trans-BET-TTF donors are 0.97, 0.33, and 0.52 eV, respectively. A calculation in which the outer five-membered rings of BET-TTF are replaced by two hydrogen atoms and keeping all other geometric details of the layer (i.e., using TTF molecules with the same inner core as the BET-TTF ones so that we completely remove the effect of the two outer S atoms) leads to values of 0.78, 0.26, and 0.40 eV. The last two calculations lead to the upper and lower values for the W, W_L, and W_U values, respectively. Of special concern here are the W_U values, i.e., the dispersion of the pair of partially filled bands. When compared with those calculated for other κ-phases using exactly the same computational approach[27,28]—for instance κ-(BEDT-TTF)$_2$Cu(NCS)$_2$ (0.59 eV), κ-(BEDT-TTF)$_2$I$_3$ (0.70 eV), κ-(MDT-TTF)$_2$AuI$_2$ (0.56 eV), and κ-(BMDT-TTF)$_2$Au(CN)$_2$ (0.74 eV)—it is clear that even the upper limit for **1** is somewhat lower than the lowest values calculated for metallic κ-phases. This suggests a strong tendency for **1** toward localization and thus activated conductivity, which is quite common for κ-phases. In the present case both the disorder in the donor layer and the lower number of holes (i.e., the average charge of the donors is +1/4 here but +1/2 in the usual κ-phases) make such localization even more likely.

Let us now briefly consider why **1** has activated but quite high electrical conductivity. There are three different types of donor···donor intermolecular interactions associated with S···S contacts shorter than 4.0 Å in the donor layers of **1**. One of them (A) is the intradimer one, whereas the other two (B and C) are associated with almost orthogonal pairs of BET-TTF donors (i.e., donors belonging to different dimers). Thus, every donor is associated with two B and two C type interactions with neighboring donors. The calculated $\beta_{HOMO-HOMO}$ intermolecular interaction energies,[29] which are a measure of the strength of the interaction between two HOMOs in adjacent sites of the layer, are 0.3302 (A), 0.1089 (B), and 0.0502 eV (C) for the ordered layer of cis-BET-TTF donors. The interdimer HOMO···HOMO interactions are clearly weaker than the intradimer one, and thus, the "natural" building blocks of the layer to house the hole are the dimers. However, since the average charge is +1/4, only half of the dimers can be described as (BET-TTF$_2$)$^+$. Because of the structural disorder, there can be several different types of dimers, i.e., trans−trans (two different types), cis−cis (two different types), and trans−cis, which are associated with intradimer $\beta_{HOMO-HOMO}$ values between 0.3481 and 0.2940 eV. This means that the site energies can vary in a nonnegligible way from one dimer to the other, and this leads to an important source of disorder from the electronic viewpoint. Then it is clear that the holes will choose to be located in half of the dimers, those associated with the largest $\beta_{HOMO-HOMO}$ values. However, the number of different possibilities of intradimer and interdimer types of interactions is too large to observe anything more than just an average structure in the crystal structure determination. However, every (BET-TTF$_2$)$^+$ dimer is surrounded by two (BET-TTF$_2$)$^+$ and two (BET-TTF$_2$)^0 dimers on average. Thus, there are large fragments of the layer that can be seen as interacting (BET-TTF$_2$)$^+$ dimers with site energies very similar to those in the usual metallic κ-phases, something that is consistent with the high but activated conductivity exhibited by **1**.

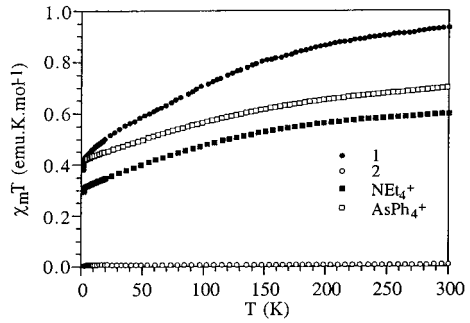

Figure 8. χ_mT vs T plot of the salt κ-(BET-TTF)$_4$(NEt$_4$)$_2$[Fe(CN)$_6$] (**1**) (filled circles), the salt (BET-TTF)$_2$[Fe(CN)$_5$NO].CH$_2$Cl$_2$ (**2**) (empty circles), and the NEt$_4^+$ (filled squares) and AsPh$_4^+$ (empty squares) salts of the [Fe(CN)$_6$]$^{3-}$ anion.

Magnetic Properties. The product of the magnetic susceptibility times the temperature (χ_mT) as a function of temperature for **1** shows at room temperature a value of 0.9 emu K mol^{-1} and a continuous decrease upon cooling to a value of ca. 0.4 emu K mol^{-1} at 2 K (Figure 8). This behavior is dominated by the magnetic properties of the [Fe(CN)$_6$]$^{3-}$ anion. In this complex the Fe(III) is in a low-spin configuration, being then described by an orbitally degenerate term $^2T_2$. This orbital contribution leads to a magnetic behavior characterized by a strong magnetic anisotropy and by a temperature-dependent χ_mT product that varies from salt to salt. In fact, with bulk cations such as NEt$_4^+$ or AsPh$_4^+$ the χ_mT product decreases from values of 0.6−0.7 emu K mol^{-1} at room temperature to values of 0.3−0.4 emu K mol^{-1} at low temperatures (Figure 8). Hence, from these magnetic susceptibility data it is very difficult to extract any information on the magnetic contribution coming from the organic sublattice. Nevertheless, an estimation of the difference between the χ_mT product of salt **1** and the NEt$_4^+$ or AsPh$_4^+$ salts of the [Fe(CN)$_6$]$^{3-}$ anion gives a constant χ_m value of $\sim 10^{-3}$ emu mol^{-1} at high temperatures (>100 K), which would come from the organic sublattice. The value of this temperature-independent paramagnetism (TIP) suggests that it can be attributed to a Pauli type paramagnetism, typical of metallic and highly conducting radical salts,[20] in agreement with the ESR data (see below).

More useful and sure information on this point can be derived from the ESR spectra. At high temperatures the [Fe(CN)$_6$]$^{3-}$ anion is ESR silent due to the short relaxation times of the $^2T_2$ term. For example, the (NEt$_4$)$^+$ salt of the [Fe(CN)$_6$]$^{3-}$ anion shows no ESR signal at high temperatures but displays a very complex spectrum with signals in the range 2000−8000 G below ca. 100 K. So, in a wide region of temperatures it is very easy to follow the signal associated with the organic radical and, by integration of the signal, to derive the magnetic susceptibility coming from this sublattice. This study shows that in the region where the inorganic anion is ESR silent (300−100 K) the susceptibility is, within experimental error, temperature independent. This TIP may be attributed to a Pauli-type paramagnetism that comes from the delocalized electrons of the organic sublattice.[20] This result indicates that the spins do not behave as localized in the organic part, in agreement with the electronic structure analysis, which indicates that in this 2D structure the (BET-TTF$_2$)$^+$ radicals are strongly interacting.

The appearance in the spectrum of the signal coming from the inorganic anion at low temperatures modifies both the line

(28) BEDT-TTF, bis(ethylenedithio)tetrathiafulvalene; MDT-TTF, (methylenedithio)tetrathiafulvalene; BMDT, bis(methylenedithio)tetrathiafulvalene.

(29) Whangbo, M.-H.; Williams, J. M.; Leung, P. C. W.; Beno, M. A.; Emge, T. J.; Wang, H.-H. *Inorg. Chem.* **1985**, *24*, 3500. These interaction energies (β) should not be confused with the conventional transfer integrals (t), although they have the same physical meaning. The β values are usually larger than the t ones mainly because overlap is included in extended Hückel calculations.

(30) Clemente-León, M. Ph.D. Dissertation, University de Valencia, Spain, 1999.

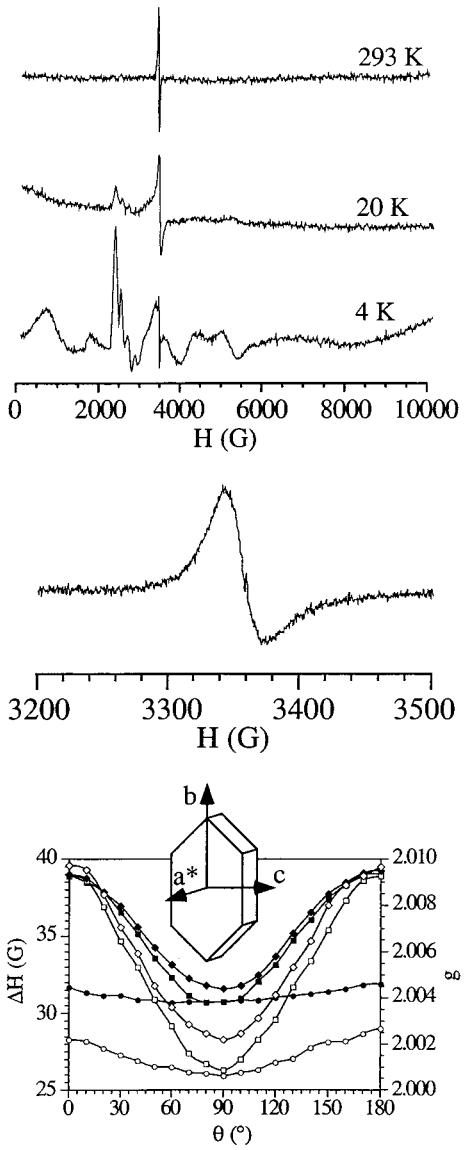

Figure 9. (top) ESR spectra of a single crystal of the salt κ-(BET-TTF)$_4$(NEt$_4$)$_2$[Fe(CN)$_6$] (**1**) at different temperatures showing the appearance of the anion signals at low temperatures. (center) ESR spectrum of a single crystal of salt **1** when the magnetic field is parallel to the *bc* plane showing the Dysonian signal coming from the BET-TTF radical. (bottom) Angular dependence of the line width (ΔH, empty symbols) and *g* factor (filled symbols) for a single crystal of salt **1** when it is rotated around the *a** (circles), *b* (squares), and *c* (rhomboids) axes. Inset: crystal orientation for the three rotations.

width and the *g* values associated with the organic sublattice (Figure 9, top). Thus, upon cooling a polycrystalline sample, the line width decreases from 40 G at room temperature to reach a minimum value of 15 G at 100 K, and below this temperature it broadens to reach a line width of ca. 60 G at 20 K and 130 G at 4 K. In a similar way the *g* factor shows a constant value of 2.009 from room temperature down to 100 K and sharply increases to 2.011 below this temperature.

Finally the ESR spectra also provide useful information on the high electron delocalization in **1**. Thus, the room-temperature ESR spectrum of a single crystal shows a Dysonian line (Figure 9, center) with A/B $\approx$ 1.7, centered at $g = 2.0038-2.0044$, with a peak-to-peak line width (ΔH_{pp}) of 26−29 G (depending on the rotation angle) when the magnetic field is parallel to the plane of the organic donors (*bc* plane), and a symmetrical line centered at $g = 2.0038-2.0093$ with a $\Delta H_{pp} = 26-40$ G (depending on the rotation angle) when the magnetic field is out of this plane (Figure 9, bottom). This Dysonian shape is typical of radical salts with high conductivity values and agrees with the fact that the best developed face of the single crystal is parallel to the *bc* plane. Moreover, the angular dependence of the *g* factor and line width of the ESR signal indicates a much smaller anisotropy when rotating the single crystal around the *a** axis (keeping the magnetic field parallel to the layers) than when the rotation is done around the other two axes (Figure 9, bottom), in agreement with the expected behavior for the 2D donor layers in a kappa phase. As expected, the largest value of the *g* factor and ΔH_{pp} were found when the magnetic field is parallel to the *a** axis, which runs almost parallel to the long axes of the BET-TTF molecules.

The magnetic properties of **2** indicate that this salt is diamagnetic. This result is in full agreement with the chemical composition and structure of the compound. In fact, the $[Fe(CN)_5NO]^{2-}$ anion is diamagnetic, and the diamagnetism in the organic sublattice is consistent with the presence of spin-paired $(BET\text{-}TTF_2)^{2+}$ dimers. After correcting the susceptibility data from the diamagnetism of the sample, the magnetic properties show a constant and very weak paramagnetic contribution of $\chi_m T = 0.009$ emu K mol^{-1} in the entire temperature range (Figure 8), which corresponds to a total amount of paramagnetic impurities of 0.024 spins/mol (i.e., one isolated $BET\text{-}TTF^+$ radical every approximately 80 donor molecules). As shown by ESR, this paramagnetic contribution comes from isolated $BET\text{-}TTF^+$ impurities. Thus, a weak and narrow signal centered at $g = 2.0067$ with $\Delta H = 16$ G is observed at room temperature whose intensity increases when decreasing temperature following a Curie law.

Conclusions

The use of the donor molecule BET-TTF with the octahedral anions $[Fe(CN)_6]^{3-}$ and $[Fe(CN)_5NO]^{2-}$ has given rise to two new radical salts formulated as κ-(BET-TTF)$_4$(NEt$_4$)$_2$[Fe(CN)$_6$] (**1**) and (BET-TTF)$_2$[Fe(CN)$_5$NO]·CH$_2$Cl$_2$ (**2**). Even if both anions are very similar in shape and size, these two salts present very different stoichiometries, packing motifs, and oxidation states of the organic radicals. Thus, salt **1** constitutes the first known kappa phase of the BET-TTF donor, whereas salt **2** presents an original structure where the anions occupy the tunnels formed by dimers of organic molecules. These differences can be attributed on one side to the different anionic charge and on the other side to the different synthetic strategy used for each salt. Thus, the use of low-soluble salts of the anion gives rise to high oxidation states (+1) in the organic donor of salt **2** as a consequence of the high applied potentials during the electroxidation of the donor. When using a very soluble salt of the anion, the oxidation state of the donor in salt **1** was much lower (1/4). The electronic spectra confirm the presence of a mixed valence state in the organic donors of salt **1** that gives rise to a high room-temperature conductivity in contrast with the low value for salt **2**, where all the donor molecules are completely oxidized. The thermal variation of the static magnetic susceptibility of salt **1** suggests the presence of a small Pauli type paramagnetic contribution at high temperatures coming from the electronic delocalization in the organic sublattice. This contribution is confirmed by the dynamic susceptibility obtained from the thermal variation of the ESR spectrum. Salt **2** is diamagnetic, in agreement with the X-ray structure (that shows a strong dimerization in the organic sublattice) and with the diamagnetic nature of the anion.

Acknowledgment. This work was supported by the M.C.T. and the DGES-Spain (Projects MAT98-0880, PB96-0872, and PB96-0859), by the Generalitat de Catalunya (Projects 1999 SGR-207 and 1998 SGR-0106), and by the programs of the European Commission TMR (3MD ERBFMRX-CT980181) and COSTD14/0003/99. V.L. is grateful to the Ministerio de Educación y Cultura for a sabbatical at ICMAB, and E.R. thanks CIRIT for a Fellowship.

Supporting Information Available: One X-ray crystallographic file with the two structures reported, in CIF format, and a PDF file with the labeling schemes, crystal data and refinement parameters, atomic coordinates, bond lengths and angles, anisotropic displacement parameters (*U*'s), and hydrogen coordinates for both structures are available on the Internet only. This material is available free of charge via the Internet at http://pubs.acs.org.

IC001431L